NANO LETTERS

pubs.acs.org/NanoLett Letter

Bamboo-like Vortex Chains Confined in Canals with Suppressed Superconductivity and Standing Waves of Quasiparticles

Wen Duan,† Kailun Chen,† Wenshan Hong, Xiaoyu Chen, Shiliang Li, Huiqian Luo,* Huan Yang,* and Hai-Hu Wen*

Cite This: *Nano Lett.* 2022, 22, 9450−9456 Read Online

ACCESS | Metrics & More | Article Recommendations | Supporting Information

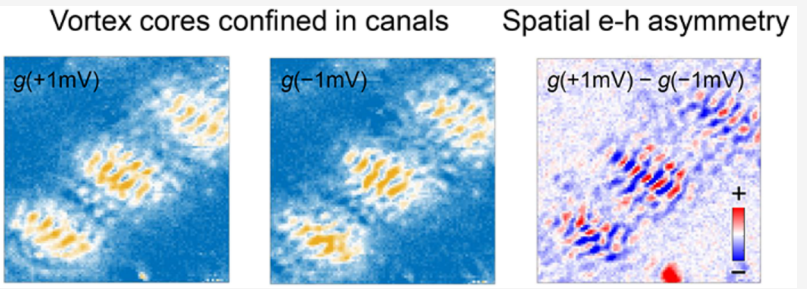

ABSTRACT: The vortex core can be regarded as a nanoscale confined system for quasiparticles in a type-II superconductor. It is very interesting to investigate the interplay between the vortex core and other microscopic quantum confined systems. We observe band-like canals with the width of about 15 nm on the surface of $KCa_2(Fe_{1-x}Ni_x)_4As_4F_2$ (x = 0.05) by scanning tunneling microscopy. Some canals suppress superconductivity and confine parallel standing waves due to the quasiparticle interference. Upon magnetic fields being applied, some elongated vortices are formed within canals showing bamboo-like one-dimensional vortex chains. Interestingly, the confined vortex cores are elongated roughly along the perpendicular direction of canals, and the local density of states at positive and negative energies shows an in-phase oscillation at zero field; but, it becomes out-of-phase crossing the vortex cores. Our work reveals a new type of vortex patterns in confined canals and its interplay with the quasiparticle interference.

KEYWORDS: *Iron-based superconductor, nanoscale confined system, pinned vortex, bamboo-like 1D vortex chain, interplay of confined electronic states*

In a type-II superconductor, vortices are formed when the applied magnetic field is stronger than the lower critical field. There is a core with a diameter of about 2ξ (ξ is the coherence length) in the vortex. In a clean superconductor, quasiparticles will be Andreev reflected at the core boundary, forming vortex bound states (VBSs) or the so-called Caroli-de Gennes-Matricon (CdGM) states.[1] The energy levels of VBSs are argued to locate at $E_\mu = \pm\mu\Delta^2/E_F$ with Δ being the superconducting gap, E_F being the Fermi energy, and μ being the quantum number taking half and odd integers.[2] Since $E_F \gg \Delta$ in most superconductors, the energy interval Δ^2/E_F of the neighboring VBS is extremely small, and discrete VBSs are very difficult to detect.[3−6] In some iron-based superconductors, E_F of some bands is comparable with Δ; thus, they are good candidates for the observation of discrete VBSs. The clear evidence of discrete VBSs was obtained in some vortex cores in Fe(Te,Se),[7] and they were later also observed in the monolayer FeSe film[8] and $(Li_{0.84}Fe_{0.16})$OHFeSe.[9,10] In these measurements, the quantum limit condition $T/T_c \lesssim \Delta/E_F$ is satisfied, and bound-state peaks of the three lowest energy levels locate at energies being quite close to the originally predicted values,[1,2] namely, 1:3:5. However, energy levels of VBSs deviate from this widely believed ratio in a newly discovered iron-based superconductor $KCa_2Fe_4As_4F_2$ (K12442)[11,12] with novel physical properties.[13−22] The reason for this deviation is that the extreme quantum limit condition $T/T_c \ll \Delta/E_F$ is satisfied, and there is a Friedel-like oscillation in the spatial evolution of the superconducting order parameter across a vortex core.[3,11,12] Due to the repulsive force between vortices, free vortices prefer to arrange into an ordered triangular lattice when the vortex pinning effect is negligible.[23,24] However, the vortex pinning seems to be strong in iron-based superconductors, and vortices usually form a disordered lattice.[7,13−30] In addition, vortices can be easily pinned by twin boundaries[25,29,31,32] or wrinkles[33] on the surface. The interaction between vortices and defects in iron-

Received: September 5, 2022
Revised: November 22, 2022
Published: November 28, 2022

https://doi.org/10.1021/acs.nanolett.2c03490
Nano Lett. 2022, 22, 9450−9456

based superconductors is an important subject with an impact in vortex pinning problems as well as Majorana modes appearing in vortex cores due to the intrinsic topological nature of some iron-based superconductors.

Here, we carried out the scanning tunneling microscopy/spectroscopy (STM/STS) study on VBSs in $KCa_2(Fe_{0.95}Ni_{0.05})_4As_4F_2$. Some canals are observed on the surface, and they show suppressed superconductivity and confine unidirectional and parallel standing waves of quasiparticles within them. Vortices can be easily pinned by these canals forming bamboo-like one-dimensional (1D) vortex chains. Interestingly, VBSs show the phase modulation effect with obvious particle−hole asymmetry to unidirectional standing waves along the direction of the canals.

In the $KCa_2(Fe_{0.95}Ni_{0.05})_4As_4F_2$ sample, the topographic features of the top surface look like those in undoped samples;[22] i.e., there are many hollows and some chains of hollows which may be induced by vacancies of surface atoms (Figure 1a). However, tunneling spectra (Figure 1b) are very inhomogeneous in the Ni-doped sample, and they are different from very homogeneous spectra obtained in the undoped K12442 sample[22] (Supplementary Note 1). In addition, the zero-bias conductance is lifted from zero in undoped samples[22] to a finite value in the doped sample. Coherence peaks locate near about ±5.5 meV on the spectra, and the peak energy is unaffected by hollows and hollow chains (Figure 1b).

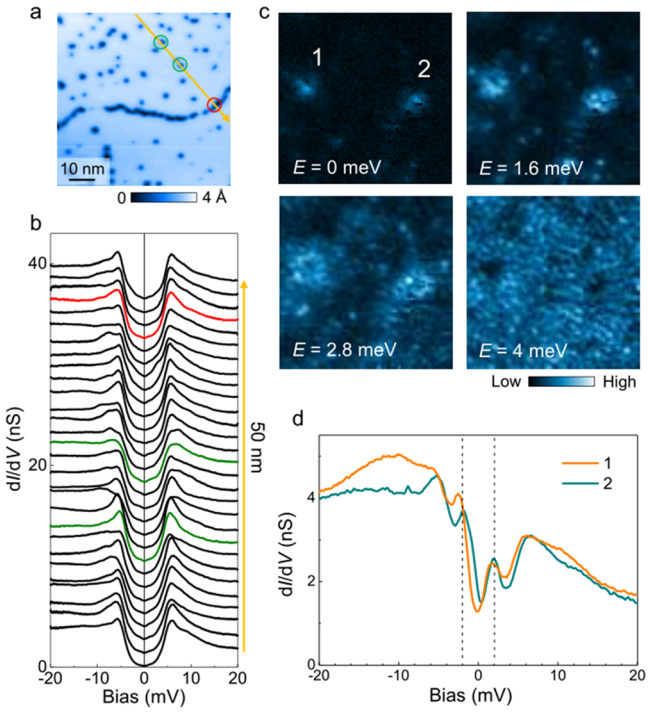

Figure 1. Vortex images and vortex bound states in $KCa_2(Fe_{0.95}Ni_{0.05})_4As_4F_2$. (a) Topographic image measured in a single crystal of $KCa_2(Fe_{0.95}Ni_{0.05})_4As_4F_2$ (Set point condition: V_{set} = 1 V, I_{set} = 20 pA). (b) A set of spatially resolved tunneling spectra measured along the arrowed line in (a). The spectra shown in olive are measured at positions of hollows on the surface, while the spectrum shown in red is measured at the position on the hollow chain. Energies of coherence peaks determined on spectra measured on hollows or hollow chains are similar to those determined on the spectra measured at other places away from these structures. (c) Vortex images measured in the same area of (a) and at different biases. The applied magnetic field is 1 T, and there are two vortex cores in the field of view. (d) Tunneling spectra measured at the centers of the two vortex cores (V_{set} = 20 mV, I_{set} = 200 pA).

In order to investigate the property of the vortex core and VBS, a magnetic field of 1 T is applied to the sample, and Figure 1c shows the differential conductance (dI/dV) mappings obtained at different energies. One can see two vortex cores in the field of view (FOV). Being different from those obtained in undoped samples,[11] the vortex images are not that clear, and Friedel oscillations of vortex cores at high energies are completely removed by the strong impurity scattering. Combined with spatially inhomogeneous tunneling spectra, there should be quite a lot of impurities in the sample which are likely to be Ni dopants. These impurities scatter quasiparticles in VBS and blur vortex images especially at high energies. However, the energy evolution of the vortex image in the Ni-doped K12442 looks roughly like that in undoped samples:[11] the vortex core behaves as a bright spot at zero bias, then becomes a bright ring at a higher energy, and finally evolves to a dark disc at the energy near the superconducting gap. Since E_F is slightly bigger than Δ in this sample, discrete VBSs should be observed in the vortex core. There are peaks of VBSs locating at about ±1.9 meV on the spectra measured at core centers (Figure 1d), and this energy is much larger than 0.8 or 0.9 meV obtained in the undoped sample.[11] In this area on the Ni-doped sample, the superconducting gap increases to 5.5 meV from 4.6 meV in the undoped sample, while E_F is slightly decreased to about 20 ± 4 meV (Supplementary Figure S2) from 24 ± 6 meV in the undoped sample.[22] Therefore, the increase of the first bound-state energy $E_{\pm 1/2} = \pm\Delta^2/2E_F$ can be explained as the Ni doping. However, impurity induced bound states also locate at about ±2 meV, and there may be a possibility that VBSs are affected by the impurity bound state, leading to a similar bound-state energy.

Besides hollows and hollow chains, we also observe some band-like canals which have not been observed in the undoped sample. Figure 2a shows a topographic image in an area with two such canals, and their width (w) is ≈15 nm. In addition, the deepest place of the canal is about 0.5 Å lower than the neighboring canal-free region at different set point biases (Supplementary Figure S3), which suggests that these canals are likely to be spatially lower than the outside region. However, the topography measured in the constant-current mode contains the information on the atomic height and also the local density of states (LDOS),[34] and we cannot conclude that the LDOS has no influence on the altitude of the canal. Nevertheless, the atomically resolved topography shows a continuous surface lattice across a canal without any visible distortions or misalignments (Supplementary Figure S4), which suggests that the canal is not the twin boundary or the dislocation of K/Ca atoms on the top surface. We notice that some wrinkles are observed on the top Li surface in LiFeAs.[33] They are a little higher than the wrinkle-free region, but the Li lattice is continuous and perfect across wrinkles. The authors attribute them to the release of the local strain during the creation of the top surface upon cleavage.[33] Since canals observed here have not been detected in undoped samples, they may be induced by the residual strain and thus slight distortion in the FeAs layer caused by Ni dopants.

As mentioned above, hollow chains on the surface have a negligible influence on the superconducting gap. However, some canals can suppress superconductivity significantly. Coherence peak energy obviously shrinks on the spectra

https://doi.org/10.1021/acs.nanolett.2c03490
Nano Lett. 2022, 22, 9450−9456

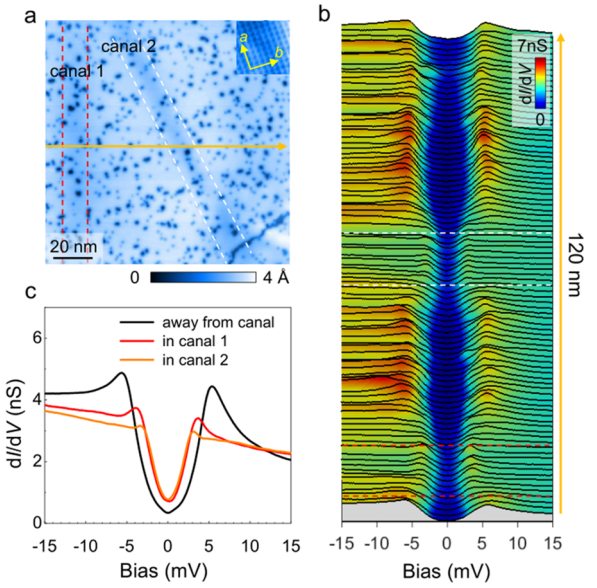

Figure 2. Canals and suppression of superconductivity. (a) Topographic image recorded in an area with two canals which are highlighted by two pairs of dashed lines (V_{set} = 1 V, I_{set} = 20 pA). The inset shows the atomically resolved topography with dimensions of 5 nm × 5 nm measured near the region shown in the main panel (V_{set} = 20 mV, I_{set} = 200 pA). (b) Spatially resolved tunneling spectra measured along the arrowed line in (a) (V_{set} = 20 mV, I_{set} = 200 pA). The spectra measured in canals are roughly indicated by two pairs of dashed lines. (c) Average curves of tunneling spectra selected from (b) measured in two canals and in the canal-free region, respectively. Since tunneling spectra are spatially inhomogeneous, we average 10 spectra measured within two canals and 30 spectra in the canal-free region and show the averaged spectra in (c).

measured within canals (Figure 2b) from about 5.5 to 3.7 meV for canal 1 and to 3.2 meV for canal 2 (Figure 2c). dI/dV at zero bias is also lifted on the spectra measured within canals, which suggests the increase of the ungapped quasiparticles. It should be noted that the angle is very small between these canals and the a-axis of the surface (also the Fe−Fe direction in the FeAs layer) determined from the atomically resolved topography (inset of Figure 2a), i.e., 18° for canal 1 and −10° for canal 2. In fact, we can also observe some canals which have a negligible influence on the superconductivity, when the angle is large between the canal and the lattice axis on the surface. Two examples are shown in Supplementary Figure S5, and the angles are 30−40° and 40−50° between the canals and the a-axis (or Fe−Fe direction). We are aware that there are two kinds of wrinkles with similar topographies on the top surface of LiFeAs, and they have different influences on the superconductivity. The difference arises from the angle between the wrinkle and the Fe−Fe direction, and the deviating angle is about 20° with respect to the Fe−Fe direction.[33] Here, in the Ni-doped K12442, canals are likely to weaken the superconductivity when they are along directions closer to the Fe−Fe direction, but they may have a negligible influence on the superconductivity when they are along directions closer to the Fe−As−Fe direction. However, since only a very limited number of canals can be observed from our experiments, this conclusion does not have statistical meaning and serves only as a preliminary one.

The lift of dI/dV by the canals makes them observable in the dI/dV mapping at zero bias (Figure 3a). Canals have the nearly constant width of about 15 nm which is much larger than $\xi \approx$ 3 nm (Supplementary Figure S6). In FeSe, the effective length of low-energy quasiparticle excitations by the twin boundary is also 1 order of magnitude larger than ξ,[31] which is similar to

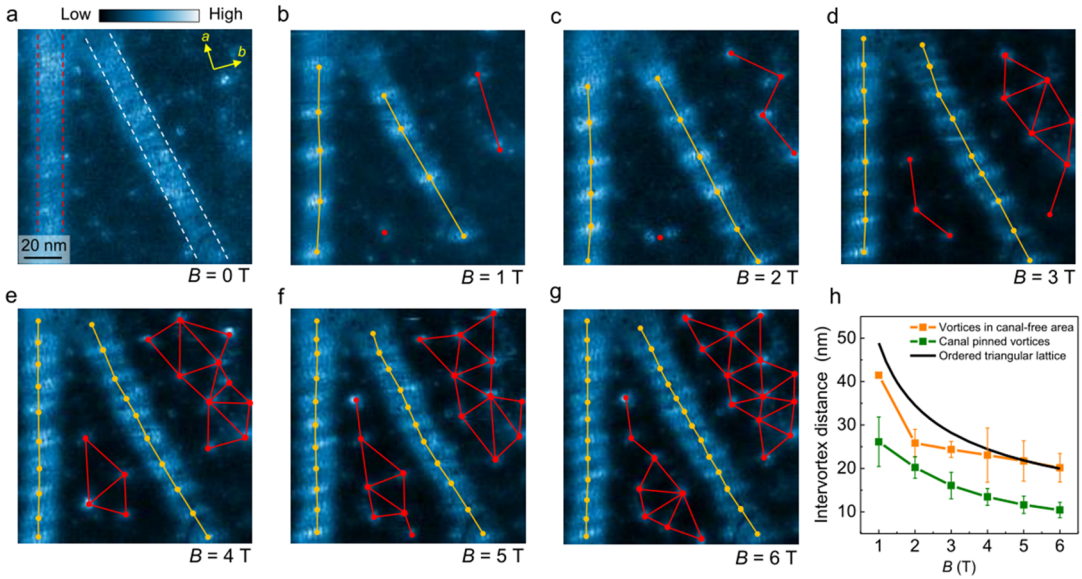

Figure 3. Vortices pinned by canals and in the canal-free region. (a−g) Differential conductance mappings measured in the same area of Figure 2a at zero bias and under different magnetic fields (V_{set} = 20 mV, I_{set} = 200 pA). Canals show up due to the lift of the zero-bias differential conductance. In the presence of the magnetic field, vortices appear in the FOV as shown in (b−g). Red dots indicate the positions of vortices staying away from the canals, while yellow dots indicate the positions of vortices pinned by the canals. Nearest neighbor dots of the same family are connected by solid lines from which we can obtain the intervortex distance. (h) Magnetic field dependence of the averaged intervortex distance for vortices pinned by canals or in the normal region far away from canals in the FOV. Error bars are calculated from the standard error of the mean. The black line shows the field dependent lattice constant calculated for an ordered hexagonal vortex lattice based on the formula $a_h = (4/3)^{1/4}(\Phi_0/B)^{1/2}$ with Φ_0 being the quantized magnetic flux.

https://doi.org/10.1021/acs.nanolett.2c03490
Nano Lett. 2022, 22, 9450−9456

the case of canals here. Besides canals, we can see some finite LDOS of the bound state induced by impurities in the canal-free region. Figure 3b–g shows dI/dV mappings at zero bias and under different fields. In the canal-free region, the distribution of vortices is very disordered, which suggests a strong pinning effect by local impurities. In addition, vortices intend to locate in canals due to the pinning effect, and these vortex cores behave as bright spots in canals which are already brighter than the surrounding canal-free area. The vortex pinning effect by canals is similar to that by twin boundaries which also suppress superconductivity in FeSe.[31,32] In the Ni-doped K12442 sample, the pinned vortex cores in a canal form a bamboo-like 1D vortex chain. By taking a close look, vortex cores are elongated roughly along the perpendicular direction of the canals, and the elongating direction tilts a bit to the b-axis of the surface lattice. Due to the pinning effect by the canals, the averaged intervortex distance decreases evidently when compared to that for vortices in the canal-free region (Figure 3h). Although vortices are disordered in canal-free areas, the averaged intervortex distance is close to the calculated lattice constant for the standard hexagonal vortex lattice, especially under high fields. Under low fields, the relatively smaller averaged intervortex distance may be due to the strong pinning effect by the canals, and the amount of vortex cores is small in the canal-free region. However, the number of vortices counted in the FOV is quite close to the theoretically expected value at the same magnetic field (Supplementary Figure S7), which suggests that the pinned vortices are also full ones, i.e., each carrying one flux quantum.

Usually, the shape of the vortex core changes when it is pinned by stripe-like pinning centers.[31−33,35] In order to investigate the detailed structure of the canal and pinned vortex cores, we carry out the dI/dV mapping in a small region. Figure 4a–c shows mappings measured at 0 T. Many parallel standing waves can be seen along the direction of the canal. They are not very clear at 0 meV because most of quasiparticles are gapped. Figure 4d–f shows dI/dV mappings

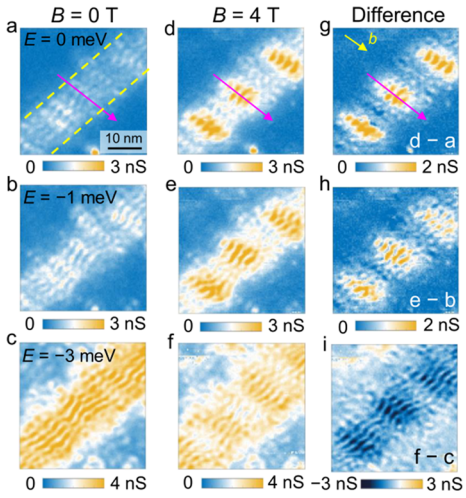

Figure 4. Vortex cores confined in the canal. (a–c) Differential conductance mappings $g(\boldsymbol{r},B = 0\ \mathrm{T})$ measured at different biases (V_{set} = 20 mV, I_{set} = 200 pA). The yellow dashed lines in (a) mark the boundaries of the canal. (d–f) Differential conductance mappings $g(\boldsymbol{r},B = 4\ \mathrm{T})$ measured at different biases (V_{set} = 20 mV, I_{set} = 200 pA). (g–i) Difference mappings of $\Delta g(\boldsymbol{r}) = g(\boldsymbol{r},B = 4\ \mathrm{T}) - g(\boldsymbol{r},B = 0\ \mathrm{T})$.

measured at 4 T, and bamboo-like vortex chains can be seen in the canal accompanied by the stripe-like standing waves, especially in Figure 4d,e. The diameter of these vortex cores is about $2\xi \approx 6$ nm in the direction along the canal; but it is equal to $w \approx 15$ nm in the perpendicular direction to the canal. In order to see the detailed structure of elongated vortex cores more clearly, we subtract dI/dV mappings measured at 0 T from those measured at 4 T in order to get difference mappings (Figure 4g–i). The enhanced dI/dV at energies of 0 and −1 meV is from the VBS in the vortex core, while the reduced dI/dV in the vortex core at −3 meV is due to the suppression of the coherence peak to a relatively low value under a magnetic field. One can see that the elongating direction is not strictly along the perpendicular direction to the canal but tilts a bit to the b-axis direction (Figure 4g).

In order to investigate the electronic structure of the parallel standing waves, we show in Figure 5a a set of tunneling spectra measured across the canal at 0 T. Friedel oscillations of LDOS can be clearly seen at high energies above 1 meV. Here at $\pm\Delta \approx \pm 3$ meV, LDOS and its spatial oscillation reach their maxima. We also plot the spatial evolution of dI/dV at ±3 meV in Figure 5c, and the obtained spatial periodicity (λ) is ≈2.1 nm. This value corresponds to a wave vector of about $0.30\pi/a_0$ which is larger than the scattering wave vector of $2k_F \approx 0.19\pi/a_0$ in the canal-free region (Supplementary Figure S2). Therefore, canals do modify the electronic structure of the material. A canal can be regarded as the combination of two 1D defects on the canal boundaries, and one-direction standing waves[36] form in the region within the canal. The amplitude of Friedel oscillations keeps a similar amplitude for the central four peaks, and then, it significantly decreases to zero near canal boundaries. Therefore, the canal can form a quasi-1D system of quasiparticles confined by two boundaries which may be induced by the mismatch of the electronic structure of neighboring materials. Nevertheless, Friedel oscillations are almost particle–hole symmetric; i.e., dI/dV at ±3 meV reaches the local extremum almost at the same position (Figure 5c).

The bamboo-like vortex chain appears in the canal at B = 4 T, and the standing waves become clearer within the elongated vortex core at energies near the VBS. Peaks of the VBSs can be seen at about ±1.5 meV on some spectra (Figure 5b), and the peak intensity of the VBS also has a spatial oscillation. However, such an oscillation is absent in a set of spectra measured across a vortex core in the canal-free area (Supplementary Figure S8). In addition, being different from the spatial evolution of the coherence-peak intensity at zero field, the peak intensity of the VBS at positive or negative energies reaches the local maximum at different positions. This phenomenon is clearer in spatial evolutions of dI/dV measured at ±1.5 meV (Figure 5d), and it also induces the spatial sign change of the difference mapping $\Delta g(\boldsymbol{r},|E|) = g(\boldsymbol{r},+E) - g(\boldsymbol{r},-E)$ across the vortex core in the elongated direction (Figure 5f, Supplementary Figure S9), but this sign change cannot be observed in the difference mapping at 0 T (Figure 5e, Supplementary Figure S9).

The shape of a vortex core can be affected by the structure of the superconducting gap,[37] and the vortex core can show an anisotropic feature when the gap or the Fermi surface is anisotropic.[27,38−42] Being different from the nearly isotropic shape of the vortex core in the canal-free region, the pinned vortex cores are elongated in the direction roughly perpendicular to the canal. It should be noted that the canal is only confined within two boundaries, and there seems no

https://doi.org/10.1021/acs.nanolett.2c03490
Nano Lett. 2022, 22, 9450−9456

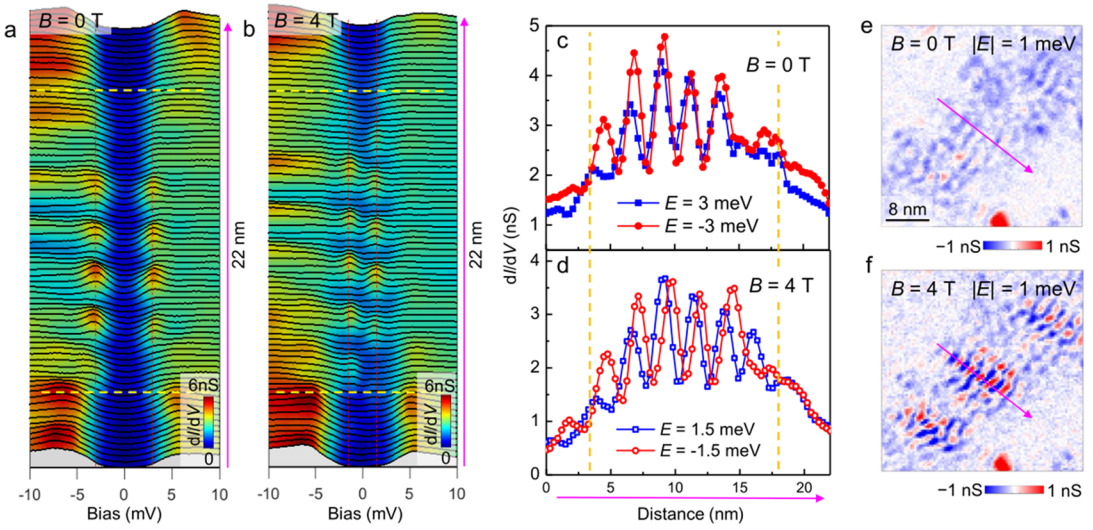

Figure 5. Interplay of the vortex bound state and canal confined state. (a, b) Spatially resolved tunneling spectra measured along the arrowed line in Figure 4a,d under the magnetic fields of 0 and 4 T, respectively (V_{set} = 20 mV, I_{set} = 200 pA). (c, d) Spatial dependence of dI/dV extracted at the bias of ±3 mV (B = 0 T) for (a) and ±1.5 mV (B = 4 T) for (b), respectively. (e, f) Difference mappings $\Delta g(\boldsymbol{r},|E|) = g(\boldsymbol{r},E = 1\ \text{meV}) - g(\boldsymbol{r},E = -1\ \text{meV})$ derived from the data obtained at 0 and 4 T, respectively.

restriction for ending points along the direction of the canal. Therefore, vortex cores have the intrinsic size of $2\xi \approx 6$ nm in the direction along the canal, but they have a diameter limited by the canal width $w \approx 15$ nm in the direction perpendicular to the canal. This shape can basically exclude the possibility that the observed vortices are Josephson ones.[43−45] Besides, the vortex core can also be regarded as a confined system, and the confined range is extended to w in the perpendicular direction. The increment of ξ in this direction can be simply understood as the increase of k_F (or the Fermi vector v_F) and decrease of Δ based on the formula $\xi = \hbar v_F/\pi\Delta$. However, it remains to be understood why pinned vortices are elongated along the perpendicular direction of the canals.

The other interesting property of the pinned vortex core is that unidirectional Friedel oscillations change the phase and show particle−hole asymmetry within the vortex core. The spatial shift is about $(0.32 \pm 0.12)\lambda$ based on Figure 5d. The spatially periodic variation of the particle−hole asymmetry is different from the axial electron−hole asymmetry of the vortex core due to its coupling to nearby magnetic impurities.[46] It should be noted that the discrete VBS is observed in both Ni-doped and undoped[11] samples, because E_F is small, and therefore, the quantum limit is satisfied in this family of materials. Based on the theoretical calculation,[3,12] although energies of the VBSs are symmetric to the zero energy, Friedel oscillations have very different spatially dependent behaviors for the VBSs with the same $|\mu|$ at positive and negative energies. For example, when a superconducting gap opens in an electron pocket, the maximum amplitude of the LDOS at $E_{+1/2}$ just appears at the core center, while that at $E_{-1/2}$ appears at a distance away from the core center (Supplementary Figure S10). The oscillations of the LDOS are almost antiphase for spatial evolutions of the LDOS at $E_{\pm 1/2}$. Therefore, such particle−hole asymmetry affects the phase of Friedel oscillations in the vortex core pinned by the canal.

To summarize, we have investigated vortex bound states in $KCa_2(Fe_{0.95}Ni_{0.05})_4As_4F_2$ by STM/STS. Some band-like canals are observed on the cleaved surface without any obvious change of the atomic lattice. The superconductivity is clearly suppressed in some canals when their directions are close to the main axes of the surface lattice or the Fe−Fe direction in the FeAs layer. Standing waves can be observed parallel to the canal boundaries. Under a magnetic field, vortices can be pinned by these canals forming bamboo-like 1D vortex chains. The core size of a pinned vortex is extended from about $2\xi \approx 6$ nm to the canal width of about 15 nm in the direction roughly perpendicular to the canal. Furthermore, Friedel oscillations become out-of-phase at energies of VBSs in the positive and negative side while it is in-phase for the oscillations at zero field. Our results provide important information on the complex interaction between electronic states of quasiparticles confined by a vortex core and those confined within the quasi-1D canal.

METHODS

The Ni-doped $KCa_2Fe_4As_4F_2$ single crystals used in this work were grown by the self-flux method.[17] Ni atoms are doped to the superconducting FeAs layer (Supplementary Figure 1a). The nominal doping level is $x = 0.05$ in $KCa_2(Fe_{1-x}Ni_x)_4As_4F_2$, and T_c is suppressed to 28 K by the Ni doping from 33.5 K in the pristine sample (Supplementary Figure 1b). STM/STS measurements were carried out in a scanning tunneling microscope (USM-1300, Unisoku Co., Ltd.). Ni-doped samples were cleaved at about 77 K in an ultrahigh vacuum with the base pressure of about 1×10^{-10} Torr, and then, they were quickly transferred to the microscope head which was kept at a low temperature. PtIr tips were used for STM/STS measurements. A typical lock-in technique was used in tunneling spectrum measurements with an ac modulation of 0.1 mV and a frequency of 931.773 Hz. Voltage offsets were carefully calibrated before STS measurements. All measurements were carried out at 1.7 K.

ASSOCIATED CONTENT

Supporting Information

The Supporting Information is available free of charge at https://pubs.acs.org/doi/10.1021/acs.nanolett.2c03490.

https://doi.org/10.1021/acs.nanolett.2c03490
Nano Lett. 2022, 22, 9450−9456

Characterization of superconductivity and surface topology, Fermi surface structure, structural and electronic properties of canals, detailed electronic structure of vortex cores, and statistics on the vortex number (PDF)

AUTHOR INFORMATION

Corresponding Authors

Hai-Hu Wen − *National Laboratory of Solid State Microstructures and Department of Physics, Center for Superconducting Physics and Materials, Collaborative Innovation Center for Advanced Microstructures, Nanjing University, Nanjing 210093, China;* orcid.org/0000-0003-0093-1625; Email: hhwen@nju.edu.cn

Huan Yang − *National Laboratory of Solid State Microstructures and Department of Physics, Center for Superconducting Physics and Materials, Collaborative Innovation Center for Advanced Microstructures, Nanjing University, Nanjing 210093, China;* orcid.org/0000-0002-6665-0327; Email: huanyang@nju.edu.cn

Huiqian Luo − *Beijing National Laboratory for Condensed Matter Physics, Institute of Physics, Chinese Academy of Sciences, Beijing 100190, China; Songshan Lake Materials Laboratory, Dongguan, Guangdong 523808, China;* Email: hqluo@iphy.ac.cn

Authors

Wen Duan − *National Laboratory of Solid State Microstructures and Department of Physics, Center for Superconducting Physics and Materials, Collaborative Innovation Center for Advanced Microstructures, Nanjing University, Nanjing 210093, China*

Kailun Chen − *National Laboratory of Solid State Microstructures and Department of Physics, Center for Superconducting Physics and Materials, Collaborative Innovation Center for Advanced Microstructures, Nanjing University, Nanjing 210093, China*

Wenshan Hong − *Beijing National Laboratory for Condensed Matter Physics, Institute of Physics, Chinese Academy of Sciences, Beijing 100190, China; School of Physical Sciences, University of Chinese Academy of Sciences, Beijing 100190, China*

Xiaoyu Chen − *National Laboratory of Solid State Microstructures and Department of Physics, Center for Superconducting Physics and Materials, Collaborative Innovation Center for Advanced Microstructures, Nanjing University, Nanjing 210093, China*

Shiliang Li − *Beijing National Laboratory for Condensed Matter Physics, Institute of Physics, Chinese Academy of Sciences, Beijing 100190, China; School of Physical Sciences, University of Chinese Academy of Sciences, Beijing 100190, China; Songshan Lake Materials Laboratory, Dongguan, Guangdong 523808, China*

Complete contact information is available at: https://pubs.acs.org/10.1021/acs.nanolett.2c03490

Author Contributions

†W.D. and K.C. contributed equally to this work.

Notes

The authors declare no competing financial interest.

ACKNOWLEDGMENTS

This work was supported by National Key R&D Program of China (Grants 2022YFA1403201 and 2018YFA0704200), the Strategic Priority Research Program (B) of Chinese Academy of Sciences (Grant XDB25000000), National Natural Science Foundation of China (Grants 12061131001, 11974171, 11927809, 11822411, and 11961160699), Beijing Natural Science Foundation (Grant JQ19002), and the Youth Innovation Promotion Association of CAS (Grant 2016004).

REFERENCES

(1) Caroli, C.; De Gennes, P. G.; Matricon, J. Bound Fermion states on a vortex line in a type II superconductor. *Phys. Lett.* **1964**, *9*, 307−309.

(2) Kramer, L.; Pesch, W. Core structure and low-energy spectrum of isolated vortex lines in clean superconductors at $T \ll T_c$. *Z. Phys.* **1974**, *269*, 59−64.

(3) Hayashi, N.; Isoshima, T.; Ichioka, M.; Machida, K. Low-lying quasiparticle excitations around a vortex core in quantum limit. *Phys. Rev. Lett.* **1998**, *80*, 2921.

(4) Gygi, F.; Schluter, M. Self-consistent electronic structure of a vortex line in a type-II superconductor. *Phys. Rev. B* **1991**, *43*, 7609−7621.

(5) Hess, H. F.; Robinson, R. B.; Waszczak, J. V. Vortex-core structure observed with a scanning tunneling microscope. *Phys. Rev. Lett.* **1990**, *64*, 2711−2714.

(6) Berthod, C. Vorticity and vortex-core states in type-II superconductors. *Phys. Rev. B* **2005**, *71*, 134513.

(7) Chen, M.; Chen, X.; Yang, H.; Du, Z.; Zhu, X.; Wang, E.; Wen, H. H. Discrete energy levels of Caroli-de Gennes-Matricon states in quantum limit in $FeTe_{0.55}Se_{0.45}$. *Nat. Commun.* **2018**, *9*, 970.

(8) Chen, C.; Liu, Q.; Bao, W. C.; Yan, Y.; Wang, Q. H.; Zhang, T.; Feng, D. Observation of discrete conventional Caroli-de Gennes-Matricon states in the vortex core of single-layer $FeSe/SrTiO_3$. *Phys. Rev. Lett.* **2020**, *124*, 097001.

(9) Zhang, T.; Bao, W.; Chen, C.; Li, D.; Lu, Z.; Hu, Y.; Yang, W.; Zhao, D.; Yan, Y.; Dong, X.; Wang, Q.-H.; Zhang, T.; Feng, D. Observation of distinct spatial distributions of the zero and nonzero energy vortex modes in $(Li_{0.84}Fe_{0.16})OHFeSe$. *Phys. Rev. Lett.* **2021**, *126*, 127001.

(10) Liu, Q.; Chen, C.; Zhang, T.; Peng, R.; Yan, Y.-J.; Wen, C.-H.-P.; Lou, X.; Huang, Y.-L.; Tian, J.-P.; Dong, X.-L.; Wang, G.-W.; Bao, W.-C.; Wang, Q.-H.; Yin, Z.-P.; Zhao, Z.-X.; Feng, D.-L. Robust and clean Majorana zero mode in the vortex core of high-temperature superconductor $(Li_{0.84}Fe_{0.16})OHFeSe$. *Phys. Rev. X* **2018**, *8*, 041056.

(11) Chen, X.; Duan, W.; Fan, X.; Hong, W.; Chen, K.; Yang, H.; Li, S.; Luo, H.; Wen, H. H. Friedel oscillations of vortex bound states under extreme quantum limit in $KCa_2Fe_4As_4F_2$. *Phys. Rev. Lett.* **2021**, *126*, 257002.

(12) Fan, X.; Chen, X.; Yang, H.; Wen, H.-H. Distinct properties of vortex bound states driven by temperature. *Europhys. Lett.* **2021**, *136*, 46002.

(13) Pyon, S.; Kobayashi, Y.; Takahashi, A.; Li, W.; Wang, T.; Mu, G.; Ichinose, A.; Kambara, T.; Yoshida, A.; Tamegai, T. Anisotropic physical properties and large critical current density in $KCa_2Fe_4As_4F$ single crystal. *Phys. Rev. Mater.* **2020**, *4*, 104801.

(14) Hong, W.; Song, L.; Liu, B.; Li, Z.; Zeng, Z.; Li, Y.; Wu, D.; Sui, Q.; Xie, T.; Danilkin, S.; Ghosh, H.; Ghosh, A.; Hu, J.; Zhao, L.; Zhou, X.; Qiu, X.; Li, S.; Luo, H. Neutron spin resonance in a quasi-two dimensional iron-based superconductor. *Phys. Rev. Lett.* **2020**, *125*, 117002.

(15) Smidman, M.; Kirschner, F. K. K.; Adroja, D. T.; Hillier, A. D.; Lang, F.; Wang, Z. C.; Cao, G. H.; Blundell, S. J. Nodal multigap superconductivity in $KCa_2Fe_4As_4F_2$. *Phys. Rev. B* **2018**, *97*, No. 060509(R).

(16) Hao, J.; Hong, W.; Zhou, X.; Xiang, Y.; Dai, Y.; Yang, H.; Li, S.; Luo, H.; Wen, H.-H. Pseudogap and strong pairing induced by

incipient and shallow bands in quasi-two dimensional $KCa_2Fe_4As_4F_2$. *Phys. Rev. B* **2022**, *106*, 014523.
(17) Wang, T.; Chu, J.; Jin, H.; Feng, J.; Wang, L.; Song, Y.; Zhang, C.; Xu, X.; Li, W.; Li, Z.; Hu, T.; Jiang, D.; Peng, W.; Liu, X.; Mu, G. Single-crystal growth and extremely high H_{c2} of 12442-type Fe-based superconductor $KCa_2Fe_4As_4F_2$. *J. Phys. Chem. C* **2019**, *123*, 13925−13929.
(18) Wang, T.; Zhang, C.; Xu, L.; Wang, J.; Jiang, S.; Zhu, Z.; Wang, Z.; Chu, J.; Feng, J.; Wang, L.; Li, W.; Hu, T.; Liu, X.; Mu, G. Strong Pauli paramagnetic effect in the upper critical field of $KCa_2Fe_4As_4F_2$. *Sci. China Phys. Mech. Astron.* **2020**, *63*, 227412.
(19) Wang, Z. C.; He, C. Y.; Wu, S. Q.; Tang, Z. T.; Liu, Y.; Ablimit, A.; Feng, C. M.; Cao, G. H. Superconductivity in $KCa_2Fe_4As_4F_2$ with separate double Fe_2As_2 layers. *J. Am. Chem. Soc.* **2016**, *138*, 7856−7859.
(20) Zhang, C.; Wu, Q.-Y.; Hong, W.-S.; Liu, H.; Zhu, S.-X.; Song, J.-J.; Zhao, Y.-Z.; Wu, F.-Y.; Liu, Z.-T.; Liu, S.-Y.; Yuan, Y.-H.; Huang, H.; He, J.; Li, S.; Liu, H.-Y.; Duan, Y.-X.; Luo, H.-Q.; Meng, J.-Q. Ultrafast optical spectroscopy evidence of pseudogap and electron-phonon coupling in an iron-based superconductor $KCa_2Fe_4As_4F_2$. *Sci. China Phys. Mech. Astron.* **2022**, *65*, 237411.
(21) Wu, D.; Hong, W.; Dong, C.; Wu, X.; Sui, Q.; Huang, J.; Gao, Q.; Li, C.; Song, C.; Luo, H.; Yin, C.; Xu, Y.; Luo, X.; Cai, Y.; Jia, J.; Wang, Q.; Huang, Y.; Liu, G.; Zhang, S.; Zhang, F.; Yang, F.; Wang, Z.; Peng, Q.; Xu, Z.; Qiu, X.; Li, S.; Luo, H.; Hu, J.; Zhao, L.; Zhou, X. J. Spectroscopic evidence of bilayer splitting and strong interlayer pairing in the superconductor $KCa_2Fe_4As_4F_2$. *Phys. Rev. B* **2020**, *101*, 224508.
(22) Duan, W.; Chen, K.; Hong, W.; Chen, X.; Yang, H.; Li, S.; Luo, H.; Wen, H.-H. Single-particle tunneling spectroscopy and superconducting gaps in the layered iron-based superconductor $KCa_2Fe_4As_4F_2$. *Phys. Rev. B* **2021**, *103*, 214518.
(23) Suderow, H.; Guillamón, I.; Rodrigo, J. G.; Vieira, S. Imaging superconducting vortex cores and lattices with a scanning tunneling microscope. *Supercond. Sci. Technol.* **2014**, *27*, 063001.
(24) Hess, H. F.; Robinson, R. B.; Dynes, R. C.; Valles, J. M., Jr.; Waszczak, J. V. Scanning-tunneling-microscope observation of the Abrikosov flux lattice and the density of states near and inside a fluxoid. *Phys. Rev. Lett.* **1989**, *62*, 214−216.
(25) Fente, A.; Meier, W. R.; Kong, T.; Kogan, V. G.; Bud'ko, S. L.; Canfield, P. C.; Guillamón, I.; Suderow, H. Influence of multiband sign-changing superconductivity on vortex cores and vortex pinning in stoichiometric high-T_c $CaKFe_4As_4$. *Phys. Rev. B* **2018**, *97*, 134501.
(26) Shan, L.; Wang, Y.-L.; Shen, B.; Zeng, B.; Huang, Y.; Li, A.; Wang, D.; Yang, H.; Ren, C.; Wang, Q.-H.; Pan, S. H.; Wen, H. H. Observation of ordered vortices with Andreev bound states in $Ba_{0.6}K_{0.4}Fe_2As_2$. *Nat. Phys.* **2011**, *7*, 325−331.
(27) Hanaguri, T.; Kitagawa, K.; Matsubayashi, K.; Mazaki, Y.; Uwatoko, Y.; Takagi, H. Scanning tunneling microscopy/spectroscopy of vortices in LiFeAs. *Phys. Rev. B* **2012**, *85*, 214505.
(28) Yin, Y.; Zech, M.; Williams, T. L.; Wang, X. F.; Wu, G.; Chen, X. H.; Hoffman, J. E. Scanning tunneling spectroscopy and vortex imaging in the iron pnictide superconductor $BaFe_{1.8}Co_{0.2}As_2$. *Phys. Rev. Lett.* **2009**, *102*, 097002.
(29) Yang, H.; Shen, B.; Wang, Z.; Shan, L.; Ren, C.; Wen, H.-H. Vortex images on $Ba_{1-x}K_xFe_2As_2$ observed directly by magnetic force microscopy. *Phys. Rev. B* **2012**, *85*, 014524.
(30) Eskildsen, M. R.; Vinnikov, L. Y.; Veshchunov, I. S.; Artemova, T. M.; Blasius, T. D.; Densmore, J. M.; Dewhurst, C. D.; Ni, N.; Kreyssig, A.; Bud'ko, S. L.; Canfield, P. C.; Goldman, A. I. Vortex imaging in Co-doped $BaFe_2As_2$. *Physcia C* **2009**, *469*, 529−534.
(31) Watashige, T.; Tsutsumi, Y.; Hanaguri, T.; Kohsaka, Y.; Kasahara, S.; Furusaki, A.; Sigrist, M.; Meingast, C.; Wolf, T.; Löhneysen, H. v.; Shibauchi, T.; Matsuda, Y. Evidence for time-reversal symmetry breaking of the superconducting state near twin-boundary interfaces in FeSe revealed by scanning tunneling spectroscopy. *Phys. Rev. X* **2015**, *5*, 031022.
(32) Song, C. L.; Wang, Y. L.; Jiang, Y. P.; Wang, L.; He, K.; Chen, X.; Hoffman, J. E.; Ma, X. C.; Xue, Q. K. Suppression of superconductivity by twin boundaries in FeSe. *Phys. Rev. Lett.* **2012**, *109*, 137004.
(33) Cao, L.; Liu, W.; Li, G.; Dai, G.; Zheng, Q.; Wang, Y.; Jiang, K.; Zhu, S.; Huang, L.; Kong, L.; Yang, F.; Wang, X.; Zhou, W.; Lin, X.; Hu, J.; Jin, C.; Ding, H.; Gao, H.-J. Two distinct superconducting states controlled by orientations of local wrinkles in LiFeAs. *Nat. Commun.* **2021**, *12*, 6312.
(34) Hoffman, J. E. Spectroscopic scanning tunneling microscopy insights into Fe-based superconductors. *Rep. Prog. Phys.* **2011**, *74*, 124513.
(35) Kalisky, B.; Kirtley, J. R.; Analytis, J. G.; Chu, J. H.; Fisher, I. R.; Moler, K. A. Behavior of vortices near twin boundaries in underdoped $Ba(Fe_{1-x}Co_x)_2As_2$. *Phys. Rev. B* **2011**, *83*, 064511.
(36) Crommie, M. F.; Lutz, C. P.; Eigler, D. M. Imaging standing waves in a two dimensional electron gas. *Nature (London)* **1993**, *363*, 524.
(37) Fente, A.; Herrera, E.; Guillamón, I.; Suderow, H.; Mañas-Valero, S.; Galbiati, M.; Coronado, E.; Kogan, V. G. Field dependence of the vortex core size probed by scanning tunneling microscopy. *Phys. Rev. B* **2016**, *94*, 014517.
(38) Hayashi, N.; Ichioka, M.; Machida, K. Star-shaped local density of states around vortices in a type-II superconductor. *Phys. Rev. Lett.* **1996**, *77*, 4074.
(39) Song, C.-L.; Wang, Y.-L.; Cheng, P.; Jiang, Y.-P.; Li, W.; Zhang, T.; Li, Z.; He, K.; Wang, L.; Jia, J.-F.; Hung, H.-H.; Wu, J.; Ma, X.; Chen, X.; Xue, Q.-K. Direct observation of nodes and twofold symmetry in FeSe superconductor. *Science* **2011**, *332*, 1410.
(40) Kaneko, S.-i.; Matsuba, K.; Hafiz, M.; Yamasaki, K.; Kakizaki, E.; Nishida, N.; Takeya, H.; Hirata, K.; Kawakami, T.; Mizushima, T.; Machida, K. Quantum limiting behaviors of a vortex core in an anisotropic gap superconductor. *J. Phys. Soc. Jpn.* **2012**, *81*, 063701.
(41) Du, Z.; Fang, D.; Wang, Z.; Li, Y.; Du, G.; Yang, H.; Zhu, X.; Wen, H. H. Anisotropic superconducting gap and elongated vortices with Caroli-De Gennes-Matricon states in the new superconductor $Ta_4Pd_3Te_{16}$. *Sci. Rep.* **2015**, *5*, 9408.
(42) Chen, M.; Chen, X.; Yang, H.; Du, Z.; Wen, H. H. Superconductivity with twofold symmetry in $Bi_2Te_3/FeTe_{0.55}Se_{0.45}$ heterostructures. *Sci. Adv.* **2018**, *4*, No. eaat1084.
(43) Yoshizawa, S.; Kim, H.; Kawakami, T.; Nagai, Y.; Nakayama, T.; Hu, X.; Hasegawa, Y.; Uchihashi, T. Imaging Josephson vortices on the surface superconductor Si(111)-$(\sqrt{7}\times\sqrt{3})$-In using a scanning tunneling microscope. *Phys. Rev. Lett.* **2014**, *113*, 247004.
(44) Roditchev, D.; Brun, C.; Serrier-Garcia, L.; Cuevas, J. C.; Bessa, V. H. L.; Milošević, M. V.; Debontridder, F.; Stolyarov, V.; Cren, T. Direct observation of Josephson vortex cores. *Nat. Phys.* **2015**, *11*, 332−337.
(45) Samokhvalov, A. V.; Plastovets, V. D.; Mel'nikov, A. S. Topological transitions in electronic spectra: Crossover between Abrikosov and Josephson vortices. *Phys. Rev. B* **2020**, *102*, 174501.
(46) Park, S.; Barrena, V.; Mañas-Valero, S.; Baldoví, J. J.; Fente, A.; Herrera, E.; Mompeán, F.; García-Hernández, M.; Rubio, Á.; Coronado, E.; Guillamón, I.; Yeyati, A. L.; Suderow, H. Coherent coupling between vortex bound states and magnetic impurities in 2D layered superconductors. *Nat. Commun.* **2021**, *12*, 4668.

https://doi.org/10.1021/acs.nanolett.2c03490
Nano Lett. 2022, 22, 9450−9456